nature neuroscience

Dynamics of motion signaling by neurons in macaque area MT

Matthew A Smith[1,2], Najib J Majaj[1] & J Anthony Movshon[1]

Most neurons in macaque area MT are selective for the direction of stimulus motion. By comparing direction selectivity for gratings and plaids, we classified MT neurons as pattern direction selective (PDS) or component direction selective (CDS). We compared the time course of responses in CDS and PDS neurons in opiate-anesthetized macaques, using a rapid pseudorandom sequence of gratings and plaids that moved in different directions. On average, responses began 6 ms earlier in CDS neurons than in PDS neurons. More importantly, the pattern-selective responses of PDS neurons did not reach their fully selective state until 50–75 ms after the responses of CDS neurons had stabilized. The population motion response of MT is therefore initially dominated by component motion signals, and does not completely represent pattern motion until substantially later. The circuits that compute pattern motion take more time to finish their work than those signaling component motion.

Many studies of visual cortex concern the mean activity of neurons measured over periods of seconds, but recently the dynamics of neural response in visual cortex have drawn increased attention. Visual cortical neurons can change their response characteristics over quite brief periods, affecting such fundamental properties as orientation selectivity[1–3] and various forms of contextual modulation[4–7]. Substantial time-dependent changes in tuning have also been reported for responses to complex stimuli in V1 and in inferotemporal cortex[8–10] and to complex motion stimuli in macaque area MT/V5[11,12]. The interpretation of these dynamic variations in response pattern is somewhat controversial: some take the view that temporal variations themselves encode important aspects of visual stimuli[13], whereas others remain agnostic as to the meaning of temporal variations and use them instead to probe the neuronal circuits that give rise to selectivity[2,14]. The circuitry and response properties of MT neurons are particularly appealing for a study of this kind because these neurons have rather precise temporal response properties[15] and perform a few well-defined visual computations.

Area MT contains a high proportion of directionally selective neurons[16–19] and plays an important role in visual motion perception[20,21]. Motion processing in primate visual cortex occurs in at least two stages. The first stage, most likely located in primary visual cortex (V1), encodes orientation, spatial frequency and motion energy in a local region of space[22]. To decode more complex motion signals, a second stage takes inputs from the first stage and combines them to compute the true direction and speed of a moving stimulus. Plaid stimuli, made by adding two sinusoidal gratings with different orientations, have proved useful in probing the circuitry of these stages of motion processing. When presented with a plaid stimulus, V1 neurons signal only the direction of motion of the component gratings, and not the true direction of the pattern[17,23] (**Fig. 1a**,**b**). However, although some cells in area MT behave similarly to those in V1, others respond to the true direction of motion of the plaid stimulus[17,24] (**Fig. 1a**,**b**). The former are termed CDS and the latter PDS. The V1 neurons that project to MT are CDS[23], consistent with the idea that circuits within MT compute pattern motion and thus represent the neural substrate for the second stage of motion processing[17].

There is evidence from both psychophysics and physiology that the neural representation of two-dimensional motion evolves over tens to hundreds of milliseconds[12,25–28]. Here we report a difference in the time course of response of CDS and PDS neurons in area MT whose dynamics match recent behavioral and psychophysical data in humans[27,28], suggesting that perceptual dynamics may be closely linked to the action of MT circuits. The additional time required for pattern direction selectivity to become manifest is considerable, and suggests that pattern motion is computed by circuits that are more complex than a simple feed-forward network.

RESULTS

We recorded from 143 neurons in area MT of 11 macaque monkeys. For each neuron, we first measured responses to drifting sinusoidal gratings presented for several seconds with a blank period between stimuli. We determined the optimal direction, spatial and temporal frequency, and area for grating stimuli, and then tested the dynamics of each neuron's response over time using a novel 'streaming' stimulus. **Figure 1c** shows this stimulus schematically. For each cell, we presented a continuous sequence of drifting gratings and plaids. We interleaved gratings of 50% contrast drifting in 12 evenly spaced directions, 12 plaid stimuli created by adding together two gratings separated by 120°, and four mean gray

[1]Center for Neural Science, 4 Washington Place, New York University, New York, New York 10003, USA. [2]Present address: Center for the Neural Basis of Cognition, Carnegie Mellon University, 4400 Fifth Avenue, 115 Mellon Institute, Pittsburgh, Pennsylvania 15232, USA. Correspondence should be addressed to J.A.M. (movshon@nyu.edu).

Published online 16 January 2005; doi:10.1038/nn1382

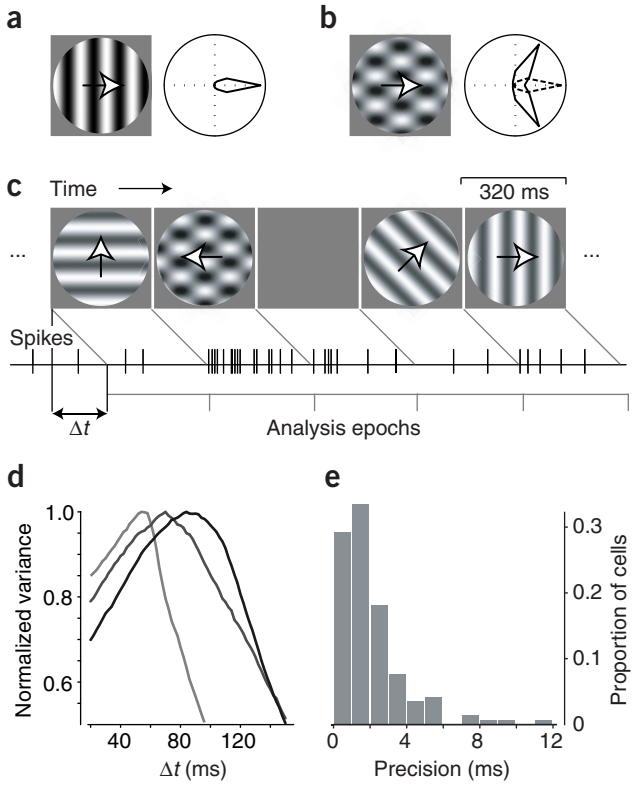

Figure 1 MT stimulus and response. (**a**) Most cells in MT are tuned for the direction of a drifting grating. A sample response is shown here in the polar plot. (**b**) When a plaid stimulus is presented, we might predict two possible responses. The pattern prediction (dotted line) is that the neuron integrates the motion signals and responds to the plaid as it does to the individual grating. The component prediction (solid line) is that the neuron responds to individual grating components of the plaid as if they were presented alone. (**c**) We used a stimulus which rapidly changed between gratings and plaids drifting in different directions. The stimulus remained on the screen, drifting, for 320 ms, after which a new stimulus was chosen randomly. This figure shows a sample sequence with a spike raster below it. Each cell has a response latency (the time it takes for a change in the stimulus to be reflected in a response change), which is indicated by Δt. We collected multiple repeats and then parsed out the response for each stimulus to arrive at a detailed response histogram. (**d**) For three sample cells, these lines represent the normalized variance in the tuning curves as a function of Δt. The peak variance values were at Δt = 56 ms, 70 ms and 84 ms. (**e**) This panel shows a frequency distribution of precision values obtained by a bootstrap method. The mean of this distribution was 2.1 ms, and 92% of the data fell below 5 ms.

blank stimuli. Every 320 ms we changed the stimulus, holding spatial and temporal frequency and size constant at the optimal values. The stimuli were presented in random order together in a block. This block was typically repeated five times (each time in a new random order), followed by several seconds of blank screen. This entire procedure was usually repeated 5–40 times to give 25–200 repetitions of each stimulus.

Determining response latency

When using a stimulus that runs continuously without pause, parsing the spike train is not as simple as with discrete, separately presented stimuli. Below the schematic stimulus in **Figure 1c** is a spike trace showing a cell's response. Because of response latency, the onset of firing induced by a stimulus lagged behind the onset of that stimulus. To relate the spikes to the stimuli that evoked them, we shifted the spike times by Δt. To optimize Δt for each cell, we computed the mean responses to all stimuli and took the variance about these means as a measure of how much of the cell's response variation could be driven by our stimuli (see Methods). **Figure 1d** shows variance as a function of Δt for three sample cells. For these and all others, the curves had a single clear maximum. We took this maximum—the value of Δt that produced the largest variance and therefore the most tuning-curve modulation—as the latency. We used a bootstrap method to compute the precision of each latency measure (see Methods) (distribution of these values is shown in **Fig. 1e**). Precision was 2.1 ms on average, and better than 5 ms for 92% of cells.

Figure 2 shows the responses of three MT cells to gratings and plaids presented with the streaming method. For each cell, average response histograms for gratings and plaids moving in different directions are shown on the right, and polar plots of response amplitude versus direction are shown on the left. The first cell (**Fig. 2a–d**) was a CDS cell, as can be seen by comparing the single-peaked tuning curve for gratings (**Fig. 2a**, gray line) with the bi-lobed tuning curve for plaids (**Fig. 2b**, gray line), whose peaks are separated by the 120° that separated the component gratings in the stimulus. The second and third cells (**Fig. 2e–h** and **i–l**, respectively) were PDS cells, as can be seen by noting the similarity of their tuning for gratings and plaids (gray curves in **Fig. 2e**,**f**,**i**,**j**). The latencies determined as detailed above for these three cells were 73 ms, 63 ms and 50 ms, indicated by the arrows beneath the response histograms. These latencies can be seen to correspond closely with the times of response onset estimated by eye from the histograms. The response details highlighted by the red and blue stripes are discussed below.

Classification of pattern and component cells

The difference between PDS and CDS cells is captured by comparing tuning for gratings with that for plaids. We took each cell's tuning curve for gratings and generated two predictions—one for a pattern response (**Fig. 1b**, dotted curve) and one for a component response (**Fig. 1b**, solid curve). We computed pattern and component correlations (R_p, R_c) of the actual response (measured over the optimal 320-ms interval determined as described above) with these predictions, using the standard technique[17,23]. These correlation measures were also converted into Z-scores using Fisher's r-to-Z transformation (see Methods). The r-to-Z transformation is a variance-stabilizing transformation that makes it possible to compute quantities such as the difference of correlation values. When using the raw correlations, the meaning of a difference between two numbers depends on their values. For example, the difference between r-values of 0.91 and 0.92 is in no meaningful sense the same as that between 0.51 and 0.52. With Z-transformation, the differences between values are in units of their standard deviation.

Figure 3 shows the distributions of both the partial correlations (R_p, R_c, **Fig. 3a**) and their Z-transforms (Z_p, Z_c, **Fig. 3b**). The class boundaries[17] separate the cells into CDS cells (blue), PDS cells (red), and intermediate or 'unclassed' cells. Approximately 25% of cells were classified as PDS (36/143) and 41% as CDS (58/143), whereas 34% were unclassed (49/143). These proportions are similar to those previously observed for this measurement in awake[29] (G. Stoner and T. Albright, personal communication; D. Bradley, personal communication) and anesthetized[17,24,30] monkeys using the same stimuli. The data in the two panels are the same, but note that the curved class boundaries in **Figure 3a** are transformed into straight lines in **Figure 3b**.

Response latency for pattern and component cells

Distributions of response latency are shown in **Figure 4a–c** for CDS, PDS and unclassed cells. PDS cells have a significantly longer latency than CDS cells by an average of about 6 ms (ANOVA, P = 0.025). The latency for PDS cells was also longer than for unclassed cells, but this

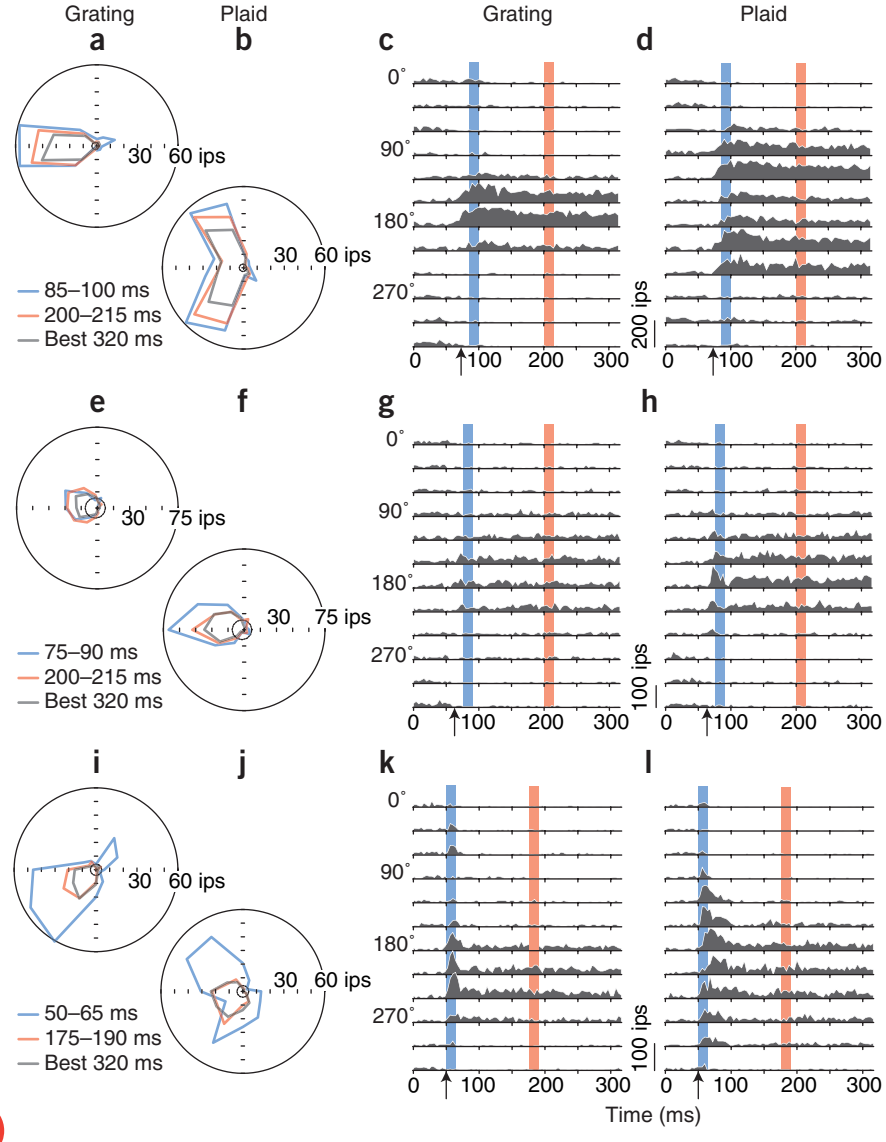

Figure 2 Three types of responses to plaids and gratings. (**a**,**b**) These two polar plots show the orientation tuning of a sample cell to gratings (left) and plaids (right). This cell had a response latency of 72.5 ms and was classified as CDS using its response from the entire 320-ms stimulus interval. The red curve indicates the cell's tuning in a 15-ms window near the beginning of the cell's response, whereas the blue curve indicates the cell's tuning in a later 15-ms window after the response has stabilized. The cell's response over a 320-ms window starting at the optimal offset is shown with the gray curve. The small black circle at center indicates the cell's baseline response to a gray screen. (**c**,**d**) These two panels show histograms of the same cell's responses to gratings (left) and plaids (right). The vertical bars indicate the early (red bar) and late (blue bar) windows from which the polar plots in **a** and **b** were taken. (**e**–**h**) These polar plots and histograms are constructed from the responses of another cell with a response latency of 62.7 ms that was classified as PDS. Like the component cell in **a**–**d**, this neuron did not show any change in its directionality to plaid stimuli over time. (**i**–**l**) Here the same plots are shown for a PDS neuron with a response latency of 50.1 ms. In this case, the cell's plaid response was markedly different over time. In the earlier window, the response matched the component prediction. In the later window, the pattern prediction was a better match for the cell's response.

difference was not statistically significant (ANOVA, $P = 0.09$). Across all cells, the mean response latency was 63.5 ± 13.9 ms, similar to that found in other studies[31–34].

Although PDS and CDS neurons show a latency difference as a group, the division of cells into those groups is based on somewhat arbitrary significance criteria. To analyze the relationship between pattern response and latency in our entire population of neurons, we computed Z_p–Z_c, which we term 'patternness', and its relationship with response latency. Across the entire population of 143 neurons, there was a significant positive correlation between 'patternness' and response latency (Pearson's $r = 0.25$, $P = 0.003$). This statistic indicates that across the full spectrum of PDS and CDS behavior, cells that tended to show more PDS behavior also tended to have longer response latencies.

The vigor and latency of cortical responses are often negatively correlated[1,33,35]. This may be because cells with very low firing rates have higher thresholds and therefore longer integration times. In the population as a whole we found a weak but significant negative correlation between peak firing rate and response latency (Pearson's $r = –0.21$, $P = 0.013$), consistent with data from other studies. Pattern, component and unclassed cells grouped separately showed correlations that were in the same direction ($r = –0.19$, –0.23, and –0.18, respectively) but were not individually significant ($P = 0.27$, 0.08, and 0.23), presumably owing to the smaller number of cells in each group. The peak firing rates of PDS cells (38.8 ± 26.4 impulses per second (ips)) and CDS cells (46.2 ± 24.0 ips) across all stimuli were not significantly different (ANOVA, $P = 0.17$). In CDS cells, the peak firing rate to grating and plaid stimuli was nearly the same (41.6 ips versus 41.4 ips). In PDS cells, the peak response to plaids (38.1 ± 26.8 ips) was much higher than to gratings (23.9 ± 13.7 ips). This difference of 12.7 ips was statistically significant (t-test, $P < 0.0001$). The baseline rates of PDS cells (4.1 ± 2.8 ips) and CDS cells (4.8 ± 4.7 ips) were very similar (ANOVA, $P = 0.40$), and there was no correlation between the spontaneous rate and response latency ($r = –0.05$, $P = 0.53$).

To assess whether the response latencies for gratings and plaids were the same for each cell, we used the same automated method to determine response latency for each neuron's responses to gratings and plaids separately (**Fig. 4d–f**). For all three classes of cells, grating and plaid latencies were highly correlated ($r = 0.90$, 0.73 and 0.88, respectively; $P < 0.0001$) but not identical. We computed the latency difference (plaid latency minus grating latency) for each class (**Fig. 4g–i**), which revealed a delay of about 4 ms for plaid response relative to grating response for PDS cells (t-test, $P = 0.006$) and unclassed cells (t-test, $P = 0.0003$). CDS cells showed a delay of 1 ms that was not statistically significant (t-test, $P = 0.43$). Across all cells, responses to gratings were on average 2.9 ± 8.5 ms earlier than responses to plaids. Cells tend to respond with shorter latencies to high-contrast stimuli[36–38]. It is notable that the response latency to plaids (100% contrast) was slightly longer than to gratings (50% contrast) even though the plaids had higher contrast, for which we might expect shorter latency responses. One simple interpretation is

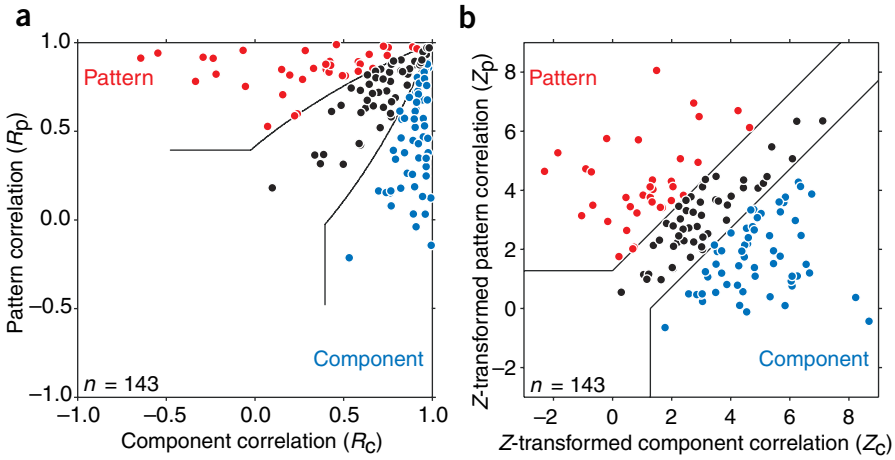

Figure 3 Pattern and component direction selectivity. (**a**) Scatter plot of R_c versus R_p used to divide MT cells into component (CDS, blue), pattern (PDS, red) and unclassed groups. The class boundaries are previously defined[17,23] and represent differences between R_c versus R_p values that have a 0.1 probability of arising by chance. (**b**) Scatter plot of Z_c versus Z_p showing data from the same calls as in **a** after applying Fisher's *r*-to-*Z* transformation to express the correlation values in units normalized by their standard deviation (Z-scores). The solid lines bound the same three plot regions as in **a**.

that latency for plaids is determined not by the pattern's total contrast, but by the contrast of each component grating, which is 50%.

Time course of response for individual neurons

The difference we found in mean response latency between PDS and CDS cells prompted us to examine the time course of response for individual cells, with the particular view of determining the selectivity of early and late parts of the response. The blue and red bars under the average response histograms in **Figures 2c** and **d**, **2g** and **h**, and **2k** and **l** indicate for each cell an early and a late response interval, respectively, of 15 ms duration, and the similarly colored curves in the polar tuning diagrams in **Figures 2a** and **b**, **2e** and **f**, and **2i** and **j** show the magnitude of response in these intervals. For the first and second examples, tuning curves taken from both windows show similar responses, indicating that these cells showed a stable direction preference for gratings and plaids over time. The third cell, however, exhibited a different response pattern (**Fig. 2i–l**). Here, the polar plots of direction tuning show the same pattern for gratings in early and late response windows (**Fig. 2i**). However, the response to plaids shows a markedly different pattern in the early and late response windows (**Fig. 2j**). Near the beginning of the response (red line), the cell behaved as a typical CDS cell would, with two peaks separated by 120° on its direction tuning curve. After the response had stabilized (blue line), the directionality for plaids was similar to that for gratings, as is characteristic of PDS cells. This change is easily seen in the average response histograms for plaids (**Fig. 2l**), where it is evident that the cell responded to a wide range of directions in the early (blue) window but showed narrower tuning in the late window. From these three examples, it is clear that some cells in area MT show dynamic changes in their direction tuning over time, whereas others maintain stable preferences throughout their responses.

To add to this qualitative view of the data, we quantitatively assessed the frequency of the two behaviors described above for pattern cells. We aligned all of the data to the response onset of each neuron and analyzed the data in 20-ms windows starting at this latency. Of the 36 neurons classified as PDS (see Methods), 9 (25%) showed significant CDS tuning (defined as a Z-score difference larger than 1.28) in the first 20-ms epoch (like the example in **Fig 2l**), whereas only 9 (25%) showed significant PDS

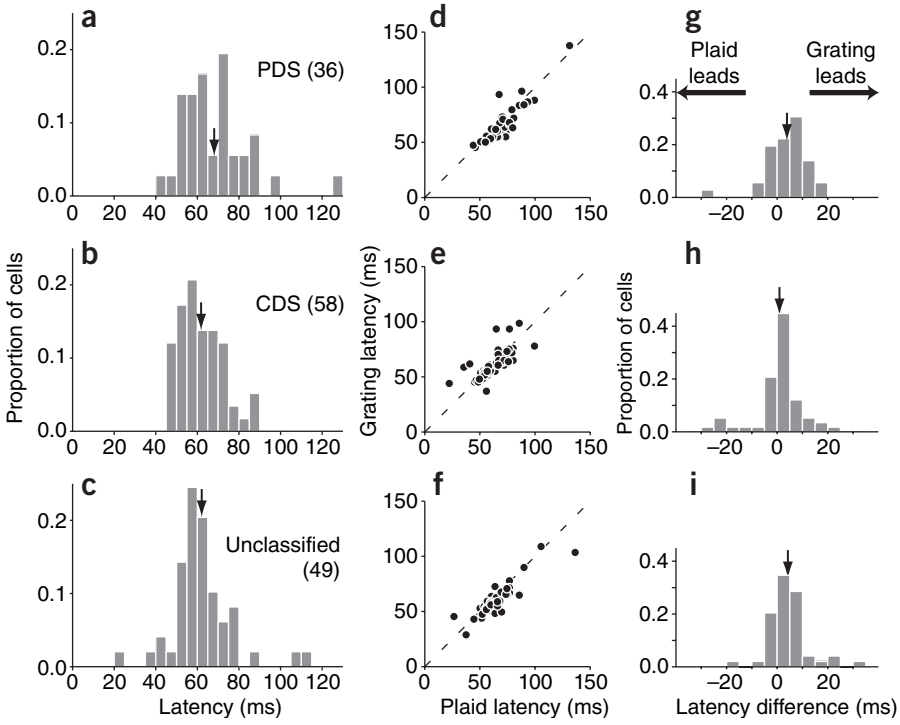

Figure 4 Response latency for pattern, component and unclassed cells. (**a**–**c**) These three PSTHs show frequency distributions of response latency in the three classes of MT neurons. The mean of each distribution is indicated with the black arrow. (**a**) Pattern cells had the longest latency on average, 68.1 ± 16.5 ms (s.d.), about 6 ms longer than for both other classes. (**b**) Component cells showed the shortest latency, 61.8 ± 10.5 ms. (**c**) Unclassed cells had an average latency that was nearly the same as for component cells, 62.3 ± 14.8 ms. (**d**–**f**) We determined the response latency separately for grating and plaid responses. These three scatter plots show these data for pattern, component and unclassed cells. (**g**–**i**) We computed the latency difference (plaid response latency minus grating response latency) for each class of cells. On average (black arrows), all cells responded earlier to gratings than to plaids, although that difference was very small: 3.9 ± 7.9 ms for pattern cells, 1.0 ± 9.2 ms for component cells and 4.3 ± 7.8 ms for unclassed cells.

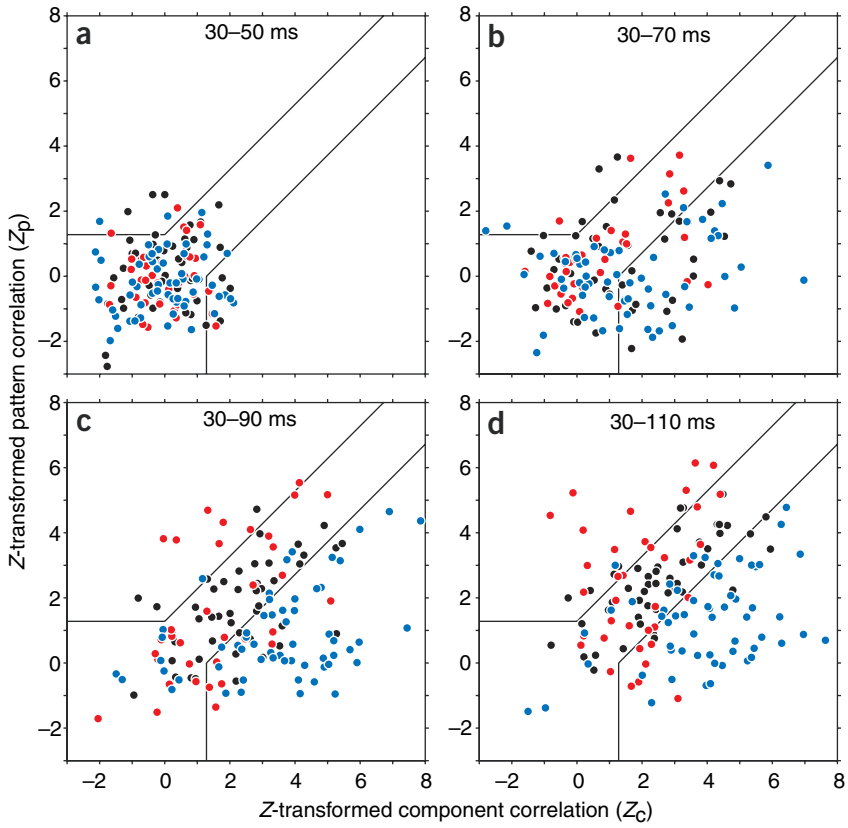

Figure 5 Scatter plot of *Z*-scores over time in sliding or cumulative windows. Here we present scatter plots of *Z*-transformed pattern and component correlation. The blue dots represent component cells, the red dots represent pattern cells, and the black dots represent those cells which are not classified. This assignment was done based on the response of the neurons over a full 320-ms stimulus window (see **Fig. 3b**). The time window ranges are indicated above each plot. (**a**–**d**) These four scatter plots show responses starting at 30–50 ms (**a**), with the cumulative window expanding by 20 ms as you move to each successive plot. The final window includes responses from 30–110 ms (**d**).

tuning (like the example in **Fig 2h**). The remaining 18 (50%) initially showed broad tuning that was not classifiable as CDS or PDS, and became PDS at variable times after response onset. For comparison, we analyzed the 58 neurons which were classified as CDS (see Methods). In the first 20 ms of response, 44 cells (76%) showed significant CDS tuning (like the example in **Fig. 2d**), whereas only 1 (2%) showed significant PDS tuning. It is clear that although the large majority of CDS cells were component selective from the very beginning of their response, most PDS cells were not pattern selective until their responses were well under way.

Population dynamics of pattern and component direction selectivity

To quantify these dynamics in our population, we generated scatter plots of *Z*-transformed pattern and component correlation for different time windows. We first classified the cells based on their responses over a full 320-ms time window (**Fig. 3**) and then plotted their responses in small time windows. The results of this type of analysis for four windows are shown in **Figure 5a–d**; cells are color-coded to indicate their selectivity in a full 320-ms window. We used a cumulative response window starting 30–50 ms after the stimulus transition (**Fig. 5a**) and extended the window by 20 ms in each successive plot. Many CDS cells (blue circles) showed early responses (that is, by the second time window (**Fig. 5b**)) that had significant component selectivity. PDS cells (red circles) tended to develop their selectivity later (**Fig. 5c–d**), and many remained unclassifiable or unselective even at the end of this long interval.

To capture the aggregate behavior of the three groups of cells, we took their mean Z_p and Z_c values for each of a series of cumulative time windows, starting with 30–35 ms and extending to 30–155 ms. A plot of Z_p against Z_c for PDS, CDS and unclassed cells is shown in **Figure 6a**. The data are connected to form a trajectory in the space of pattern and component selectivity that describes the growth of their selectivity with time after stimulus onset; the labels indicate the end of each time window plotted. CDS cells (blue line) develop their characteristic response tuning much earlier (within 60–65 ms) than do PDS cells (red line, 125–130 ms). In addition, whereas CDS cells show an increase in Z_c at very early times with little change in Z_p, in PDS cells both correlations increase for some time before Z_p dominates. This population behavior presumably reflects a general tendency, evident in some individual cells (**Fig. 2i–l**), for CDS-type responses or broadly tuned responses to predominate early in the response of many PDS and unclassed cells.

Another way to visualize this result is through the difference in the *Z*-scores for pattern and component correlation: the deviation from the diagonal in the space of **Figure 6a**. We plotted Z_c–Z_p (which one might term 'componentness') for CDS cells, and Z_p–Z_c (or 'patternness') for PDS cells, against time (**Fig. 6b**), using the same cumulative bins as in **Figure 6a**. It is again obvious that the response time courses of pattern and component cells are quite different. The horizontal black line in this figure (and the parallel black lines in **Fig. 6a**) represents the significance value we used in previous analysis (**Fig. 3**). This value is a measure of significance for an individual cell, and the plotted lines represent the *Z*-correlation of an average neuron in each class. Taking this value as a threshold, there is a difference of approximately 60–70 ms between the time at which the average CDS cell and the average PDS cell become significantly selective.

DISCUSSION

The signaling of true pattern direction by neurons in area MT is one of the hallmarks of direction selectivity in this area[17]. Our results show that this signal evolves during the first 100–150 ms after the presentation of a complex stimulus such as a plaid. CDS cells, thought to represent an earlier stage of motion processing than PDS cells, give responses whose selectivity is stable and consistent from the time they are first activated. But PDS cells often respond with different and broader selectivity when first activated, sometimes even resembling CDS cells. After some tens of milliseconds, their responses evolve to be more PDS-like. Only one CDS cell behaved analogously, first responding to the motion of the pattern and later to the motion of the components. Population analyses confirmed that PDS cells tend to develop their characteristic response more slowly than CDS cells. Although a 6-ms latency difference between the classes contributes to this effect, the tuning dynamics show a much more substantial difference than is explained by response latency alone. In other words, the computation

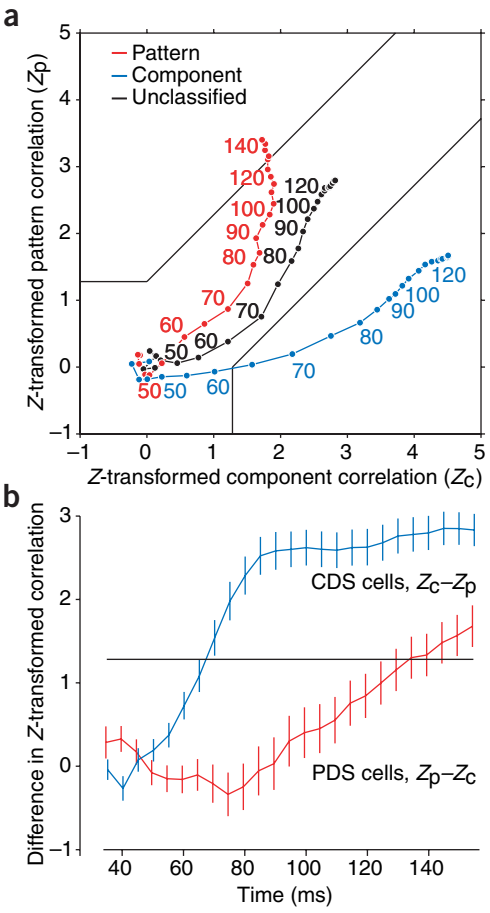

Figure 6 Line plots showing the evolution of *Z*-correlation values over time. (**a**) In this panel we show the evolution of pattern and component responses. The red line represents PDS cells, the blue line represents CDS cells, and the black line represents unclassed cells. We plotted each data point as the average value of Z_c and Z_p at that time for each class of cells. The data are analyzed cumulatively, so each point represents the *Z*-correlation for the average response from time zero up that time. The numbers along each line indicate the time of the closest data point. For example, the blue number '60' indicates that the adjacent data point represents the average value of Z_c and Z_p for component cells up to and including the time window beginning at 60 ms (and ending at 65 ms). (**b**) The evolution of the *Z*-transformed pattern and component correlation over time. Here we plot the deviation from the diagonal in the space of **Figure 6a**, which is the difference in the *Z*-scores for pattern and component correlation (Z_c–Z_p for CDS cells, plotted with a blue line, and Z_p–Z_c for PDS cells, plotted with a red line). The data points are spaced by 5 ms, and each point represents the correlation measured from a tuning curve calculated from all the data up to that time (error bars show ± 1 s.e.m.). The first point is the correlation from 30–35 ms, and the last point from 30–155 ms. The horizontal black line indicates the significance value used throughout this chapter for *Z*-correlation significance for one cell. CDS cells crossed this significance line approximately 60–70 ms earlier than PDS cells.

of pattern direction proceeds more slowly after response onset than the computation of component direction. These results suggest that cortical processing of two-dimensional motion signals by MT neurons is a dynamic process that is continuously shaped in the first hundred milliseconds of the neurons' responses.

Plaid patterns with component gratings of unequal speed have a two-dimensional 'pattern' velocity that differs in direction from the mean of the component velocities[17]. Human observers viewing these 'type 2' plaids perceive mostly component motion in brief presentations and pattern motion only after a delay[27]. The delayed selectivity of PDS neurons offers a direct explanation for this perceptual effect: the shift from perceiving component velocity to perceiving pattern velocity corresponds to a shift in population activity from an early phase dominated by the early selective response of CDS cells to a later one in which the delayed selective response of PDS cells becomes important. Although we did not use 'type 2' stimuli in our physiological experiments, one need only assume that the difference in response dynamics in our experiments is characteristic of CDS and PDS responses to other kinds of stimuli. Our data also parallel the behavior of short-latency ocular following responses to grating and plaid stimuli in human subjects[28]. With conventional plaids (made from two orthogonal moving gratings) or single gratings, motion onset elicits a very fast response closely aligned from the outset to the true motion direction. With 'unikinetic plaids' ('type 2' plaids made from one stationary and one moving grating separated by 45° in orientation), the ocular following response initially follows the grating motion and only later follows the plaid motion. This result demonstrates behaviorally that the encoding of two-dimensional motion in plaid patterns takes additional processing time compared with gratings, and agrees qualitatively with our physiological data showing that the processing of plaid patterns evolves over time.

Two recent studies have shown changes in direction preference during the responses of cells in motion-sensitive areas of cortex. One study[11] examined responses in the posteromedial lateral suprasylvian area (PMLS) of the cat evoked by fields of randomly placed iso-oriented line segments in which the angle between orientation and direction of movement was varied. The early responses tended to be more selective to orthogonal (line) motion than the later responses, which reflected the true direction. These results are broadly consistent with ours in that they show an initial predominance of component-dominated response. In area MT of the alert macaque, a stimulus of terminated bars evoked similar behavior[12]. When the bars moved obliquely to their orientation, cells initially responded to the motion of the bar segments, and only later signaled the true direction of motion. Our data show that CDS cells have shorter latencies and reach their characteristic response faster than PDS cells. CDS signals would therefore dominate the early average population response, and PDS cells would contribute later. However, the terminated line stimuli in those experiments, unlike plaid stimuli, contain motion signals that can be disambiguated by CDS neurons alone, as shown in recent imaging studies of primary visual cortex[39]. Moreover, the results of these experiments in cat PMLS and macaque MT are very similar, even though PMLS contains few, if any, PDS cells[11,12,40]. The similarity between our results and those obtained with terminated line stimuli may therefore be more illusory than real, and whether they all reflect the processes we have uncovered remains open to discussion.

It appears that the difference between the dynamics of CDS and PDS cells reflects a fundamental difference in the neural circuitry of these two cell types. What kind of circuits might account for the very substantial timing differences we observe? One model that has been proposed to account for the behavior of PDS neurons in MT is an extension of the normalization model in V1 (ref. 41). In this framework, pattern selectivity arises from a recurrent circuit that implements a divisive gain control. In principle, such a recurrent network might take some time to stabilize, and although it is stabilizing, one would expect to see the CDS-like behavior of input neurons expressed in responses, much as we observed in some PDS cells (as in **Fig 2i–l**). Such a gain control circuit is thought to act in V1, where it can be shown to act very quickly (within a few milliseconds[42]). If MT's gain control is responsible for the slow (40–60 ms) evolution of PDS responses, it

must be based on very different circuitry and involve some very slow form of recurrent inhibition not evident in V1.

A second idea is that pattern motion signals might derive from feedback from higher cortical areas, which presumably represent more advanced processing. These signals might enter MT after a delay and influence responses. The earliest responses would then reflect feed-forward processing, whereas the slower dynamics of PDS responses could reflect the influence of the feedback signal. Arguing against this idea is the likelihood that feedback signals from higher areas are attenuated under anesthesia and the evidence from studies of lower visual areas which suggests that feedback signals modulate but do not directly activate cortical neurons[43].

Another proposal is that pattern and component motion might be computed in two separate pathways, as proposed on psychophysical grounds[44]. If the 'pattern' pathway were slower, dynamics in MT might reflect the additional time needed for signals from this pathway to propagate. However, there is no obvious candidate for a separate cortical 'pattern' pathway, because studies of pattern and component selectivity in areas V2 and V3 do not suggest an important separate contribution of those areas to PDS behavior in MT[45,46].

Finally, within MT, cells might vary in their dynamics based on the position they occupy within the local cortical circuitry (for instance, input layers versus output layers). We determined the laminar location for only a fraction of our cells. Examining the laminar distribution of PDS and CDS neurons and laminar variations in latency does not reveal strong trends in the predicted direction for this subset of our data, but further experiments may prove more illuminating.

Regardless of the underlying neural mechanism, our results show a clear difference in response dynamics between two functionally distinct signals evident in neurons in a single cortical area; we are aware of no comparable difference in response dynamics in any previous work. The dynamics we observe match well with psychophysical data and are likely to be connected directly to the perception of complex motion stimuli in the natural environment. Because there are principled reasons to believe that pattern selectivity is computed directly from component selective inputs[17,23], our findings define a uniquely favorable system with which to probe the timing and architecture of cortical computation using natural stimuli.

METHODS

Electrophysiology. We recorded extracellularly from single units in area MT of seven Cynomolgus macaques (*Macaca fascicularis*), two bonnet macaques (*M. radiata*) and two pig-tailed macaques (*M. nemestrina*), ranging in weight from 4.0 to 7.9 kg. The data from all three species were indistinguishable in all respects.

The techniques used in our laboratory for recording from the visual cortex of anesthetized, paralyzed monkeys have been reported in detail elsewhere[47]. Briefly, animals were premedicated with atropine sulfate (0.05 mg kg^{-1}) and diazepam (Valium, 1.5 mg kg^{-1}) 30 min before induction of anesthesia with ketamine HCl (10.0 mg kg^{-1}). Anesthesia was maintained throughout the experiment by a continuous infusion of sufentanil citrate (typically 4 μg kg^{-1}, adjusted for each animal). Under this anesthetic regime, MT responses to grating and texture stimuli are similar in magnitude, reliability and time course to those in awake animals (L.P. O'Keefe and J.A.M., unpublished observations). To minimize eye movements, the animal was paralyzed with a continuous intravenous infusion of vecuronium bromide (Norcuron, 0.1 mg kg^{-1} hr^{-1}). Vital signs (EEG, ECG, end-tidal P_{CO2}, temperature and lung pressure) were monitored continuously. The pupils were dilated with topical atropine and the corneas protected with gas-permeable hard contact lenses. We used supplementary lenses to bring the retinal image into focus by direct ophthalmoscopy. We later adjusted the refraction further to optimize the response of recorded units. Experiments typically lasted 4–5 d. All procedures complied with guidelines approved by the New York University Animal Welfare Committee.

We recorded with quartz-platinum-tungsten microelectrodes (Thomas Recording) advanced with a mechanical microdrive through a small durotomy made within a craniotomy of approximately 10 mm diameter. The craniotomy was typically centered 4 mm posterior to the lunate sulcus and 15 mm lateral to the midline. The electrode was advanced 20° anterior and down in the parasagittal plane. MT cells were recorded at eccentricities ranging from 2° to 33°, but the great majority of cells were between 3° and 12°. Apart from the larger scale of the more peripheral receptive fields, we noticed no differences related to eccentricity. Signals from the microelectrode were amplified and bandpass filtered, and we isolated single units with a dual-window time-amplitude discriminator (Bak). The time of each action potential was recorded with a resolution of 0.25 ms by a CED-1401 Plus laboratory interface (Cambridge Electronic Design).

We made small electrolytic lesions at the end of each electrode track by passing DC current (2 μA for 5 s, tip negative) through the recording electrode. Once the experiment was finished, the animals were killed with an overdose of Nembutal and perfused through the heart with 0.1 M PBS followed by 4% paraformaldehyde in 0.1 M PBS. Sections of the superior temporal sulcus were taken every 40 μm and stained for Nissl substance with cresyl violet or myelin using Gallyas' method[48]. We were able to confirm most recording locations directly, but in some cases we relied on proximity to histologically confirmed recording sites and a high proportion of directional cells with relatively small receptive fields to determine that the recordings were made in MT[49].

Visual stimulus generation. We displayed all visual stimuli at a resolution of 1,024 × 731 pixels and a video frame rate of 100 Hz on an Eizo T550 monitor. The video monitor was placed between 80 and 180 cm from the animal's eye, where it subtended between 10° and 22° of visual angle. We used look-up tables to correct for nonlinearities in the relation between input voltage and phosphor luminance in the monitors. We generated grating stimuli for basic characterization with a Cambridge Research Systems VSG 2/2 board running on an Intel x86-based host computer. The dynamic grating and plaid stimulus was generated with a Silicon Graphics workstation. The mean luminance of the display was 33 cd m^{-2}. We presented gratings and plaids to the dominant eye in a circular aperture surrounded by a gray field of the average luminance. The starting phase was set to the same value for all stimuli. The stimuli were equal in duration (typically 1–2 s) and were separated by presentation of a uniform mean gray background for about 1.5 s. For each isolated neuron, we determined the optimal direction, spatial and temporal frequency, position and size of a 100% contrast drifting sine wave grating. After the initial characterization of each neuron with gratings, we presented a dynamic random plaid and grating stimulus. Gratings were presented at 50% contrast, and plaids were constructed by adding two such gratings separated by 120° in orientation. We presented each of these two types of stimuli drifting in 12 different directions, in addition to four periods of blank (mean gray) screen. Trials lasted 45 s and consisted of all 28 of the stimuli presented in random order for 320 ms each, with five presentations of each stimulus. These trials were typically repeated 20 times, to achieve 100 presentations of each of the 28 stimuli. The actual number of presentations was chosen for each cell based on the variability of its response (the range was 15–300).

Determining response latency. We used a novel method to determine response latency in MT neurons with our 'streaming' stimulus (**Fig. 1c**). For each neuron, we computed the mean firing rate for each of the 28 stimuli (12 gratings, 12 plaids, 4 blank screens) in a sliding window of duration 320 ms (the stimulus duration) beginning Δt ms after stimulus onset. When Δt was set at any value other than the response latency, the cell's response was not well aligned with the window used to compute the mean firing rate, and spikes due to any stimulus would spill into an adjacent analysis window, diluting differences in response and bringing the firing rate for a given interval closer to the average firing rate to all stimuli. As Δt approached the true latency, the mean firing rate increased for the preferred stimuli over the window and decreased for the non-preferred stimuli. When the value of Δt was at the true response latency, the tuning curve would have the maximum modulation, which we took as the variance of the responses to each stimulus about the overall mean. Preliminary exploration showed that the appropriate values of Δt typically fell between 40 and 100 ms; for each cell, we used a binary search method to find the optimal value in the range of 20–200 ms, within which the relationship between Δt and tuning curve variance was invariably of inverted-U shape with a single maximum.

We tested the precision of this latency estimate with a bootstrap method. For each cell, we randomly chose one-half of the presentations of each stimulus and computed the latency only using that subset of the data. We repeated this 100 times for each cell, randomly choosing a different subset of trials each time, and computed the standard deviation of the latencies. The resulting values were based on a bootstrap using only half of the trials for each cell, so we divided this number by $\sqrt{2}$ to estimate the standard error of the latency; the distribution of these values for all cells is shown in **Figure 1e**.

To test the generality of this method, we compared it with another procedure for computing latency. For 37 neurons, we collected grating and plaid tuning curves using a more conventional stimulus period of 1–2 s with a blank period of approximately 2 s between stimuli. We calculated latency for this data as the time required to reach 50% of peak response in a mass histogram of responses to all stimuli. Latency values computed in this way correlated very well with those from the streaming method (Pearson's $r = 0.53$, $P < 0.001$). The streaming method gave slightly longer latencies on average (by 4.8 ms), although this difference was not statistically significant ($P = 0.123$). We conclude that our automated method is an efficient and unbiased way to determine response latency. It is important to note that this method captures 'average' latency, but not variations in latency across stimuli. For instance, it might not work well were contrast the experimental variable, because there is a systematic variation in the time of response onset with contrast[36–38]. As response offset typically has a shorter latency than response onset[35], the method has the 'leeway' it needs to work when the latency variations across stimuli are neither large nor systematic.

Analysis of MT pattern and component data. We computed the partial correlation for the pattern and component predictions using standard methods[17]. For each cell, we used the response latency (determined using the method described above) to determine the window over which we calculated these correlations. That is, if a cell's latency was determined to be 50 ms, we calculated the correlations based on tuning curves made from responses 50–370 ms (the response latency plus the stimulus duration) after the transitions in our dynamic MT stimulus. The partial correlations for the pattern and component predictions are of the form

$$R_p = \frac{(r_p - r_c\, r_{pc})}{\sqrt{(1-r_c^2)(1-r_{pc}^2)}}$$

and

$$R_c = \frac{(r_c - r_p\, r_{pc})}{\sqrt{(1-r_p^2)(1-r_{pc}^2)}}$$

where r_c is the correlation of the data with the component prediction, r_p is the correlation of the data with the pattern prediction and r_{pc} is the correlation of the two predictions.

Because the sampling distribution of Pearson's r is not normal, we used Fisher's r-to-Z transformation for its variance-stabilizing effect. We took each value of R_p or R_c and converted it to a Z-score using the following equation (shown for R_p):

$$Z_p = \frac{0.5 \ln\left(\frac{(1+R_p)}{(1-R_c)}\right)}{\sqrt{\frac{1}{df}}}$$

where df is the degrees of freedom, equal to the number of values in the tuning curve minus 3 (there were 12 directions in our tuning curves). The numerator of the equation is the Fisher r-to-Z transformation. Each value of Z_c or Z_p was then tested for significance. We used a criterion of 1.28, equivalent to $P = 0.90$, for this purpose. For a cell to be judged as a PDS cell, the value of Z_p had to exceed the value of Z_c (or zero, if Z_c is negative) by this amount. Similarly, Z_c had to exceed Z_p by that same amount (1.28) for a cell to be judged as CDS. If a cell met neither of these conditions, it remained unclassed.

ACKNOWLEDGMENTS

This work was supported by a research grant from the NIH (EY02017), and by an HHMI Investigatorship to J.A.M. M.A.S. was supported in part by a National Eye Institute Institutional Training Grant (T32-7136). We thank A. Kohn, N. Rust and S. Schultz for assistance with some of the data collection, R. Young for technical assistance, and M. Hou and N. Doron for help with histology. We are grateful to W. Bair and A. Kohn for helpful advice and discussion.

COMPETING INTERESTS STATEMENT

The authors declare that they have no competing financial interests.

Received 9 July; accepted 10 November 2004
Published online at http://www.nature.com/natureneuroscience/

1. Celebrini, S., Thorpe, S., Trotter, Y. & Imbert, M. Dynamics of orientation coding in area V1 of the awake primate. *Vis. Neurosci.* **10**, 811–825 (1993).
2. Ringach, D.L., Hawken, M.J. & Shapley, R. The dynamics of orientation tuning in the macaque monkey striate cortex. *Nature* **387**, 281–284 (1997).
3. Ringach, D.L., Hawken, M.J. & Shapley, R. Dynamics of orientation tuning in macaque v1: the role of global and tuned suppression. *J. Neurophysiol.* **90**, 342–352 (2003).
4. Bair, W., Cavanaugh, J.R. & Movshon, J.A. Time course and time-distance relationships for surround suppression in macaque V1 neurons. *J. Neurosci.* **23**, 7690–7701 (2003).
5. Knierim, J.J. & Van Essen, D.C. Neuronal responses to static texture patterns in area V1 of the alert macaque monkey. *J. Neurophysiol.* **67**, 961–980 (1992).
6. Lee, T.S., Yang, C.F., Romero, R.D. & Mumford, D. Neural activity in early visual cortex reflects behavioral experience and higher-order perceptual saliency. *Nat. Neurosci.* **5**, 589–597 (2002).
7. Zipser, K., Lamme, V.A. & Schiller, P.H. Contextual modulation in primary visual cortex. *J. Neurosci.* **16**, 7376–7389 (1996).
8. Richmond, B.J., Optican, L.M., Podell, M. & Spitzer, H. Temporal encoding of two-dimensional patterns by single units in primate inferior temporal cortex. I. response characteristics. *J. Neurophysiol.* **57**, 132–146 (1987).
9. Richmond, B.J., Optican, L.M. & Spitzer, H. Temporal encoding of two-dimensional patterns by single units in primate primary visual cortex. I. Stimulus-response relations. *J. Neurophysiol.* **64**, 351–369 (1990).
10. Sugase, Y., Yamane, S., Ueno, S. & Kawano, K. Global and fine information coded by single neurons in the temporal visual cortex. *Nature* **400**, 869–873 (1999).
11. Li, B., Chen, Y., Li, B.W., Wang, L.H. & Diao, Y.C. Pattern and component motion selectivity in cortical area PMLS of the cat. *Eur. J. Neurosci.* **14**, 690–700 (2001).
12. Pack, C.C. & Born, R.T. Two-dimensional substructure of MT receptive fields. *Nature* **409**, 1040–1042 (2001).
13. McClurkin, J.W., Optican, L.M., Richmond, B.J. & Gawne, T.J. Concurrent processing and complexity of temporally encoded neuronal messages in visual perception. *Science* **253**, 675–677 (1991).
14. McLaughlin, D., Shapley, R., Shelley, M. & Wielaard, D.J. A neuronal network model of macaque primary visual cortex (V1): orientation selectivity and dynamics in the input layer $4c_\alpha$. *Proc. Natl. Acad. Sci. USA* **97**, 8087–8092 (2000).
15. Bair, W., Koch, C., Newsome, W. & Britten, K. Power spectrum analysis of bursting cells in area MT in the behaving monkey. *J. Neurosci.* **14**, 2870–2892 (1994).
16. Albright, T.D. Direction and orientation selectivity of neurons in visual area MT of the macaque. *J. Neurophysiol.* **52**, 1106–1130 (1984).
17. Movshon, J.A., Adelson, E.H., Gizzi, M.S. & Newsome, W.T. The analysis of visual moving patterns. in *Pattern Recognition Mechanisms* (eds. Chagas, C. Gattass, R. & Gross, C.) 117–151 (Springer, New York, 1985).
18. Van Essen, D.C., Maunsell, J.H.R. & Bixby, J.L. The middle temporal visual area in the macaque: Myeloarchitecture, connections, functional properties and topographic organization. *J. Comp. Neurol.* **199**, 293–326 (1981).
19. Zeki, S.M. Functional organization of a visual area in the posterior bank of the superior temporal sulcus of the rhesus monkey. *J. Physiol. (Lond.)* **236**, 549–573 (1974).
20. Britten, K.H., Shadlen, M.N., Newsome, W.T. & Movshon, J.A. The analysis of visual motion: a comparison of neuronal and psychophysical performance. *J. Neurosci.* **12**, 4745–4765 (1992).
21. Newsome, W.T. & Paré, E.B. A selective impairment of motion perception following lesions of the middle temporal area MT. *J. Neurosci.* **8**, 2201–2211 (1988).
22. DeValois, R.L., Albrecht, D.G. & Thorell, L.G. Spatial frequency selectivity of cells in macaque visual cortex. *Vision Res.* **22**, 545–559 (1982).
23. Movshon, J.A. & Newsome, W.T. Visual response properties of striate cortical neurons projecting to area MT in macaque monkeys. *J. Neurosci.* **16**, 7733–7741 (1996).
24. Rodman, H.R. & Albright, T.D. Single-unit analysis of pattern-motion selective properties in the middle temporal visual area (MT). *Exp. Brain Res.* **75**, 53–64 (1989).
25. Kooi, F.L., DeValois, K.K., Switkes, E. & Grosof, D.H. Higher-order factors influencing the perception of sliding and coherence of a plaid. *Perception* **21**, 583–598 (1992).
26. Lorenceau, J., Shiffrar, M., Wells, N. & Castet, E. Difference motion sensitive units are involved in recovering the direction of moving lines. *Vision Res.* **33**, 1207–1217 (1993).

27. Yo, C. & Wilson, H.R. Perceived direction of moving two-dimensional patterns depends on duration, contrast and eccentricity. *Vision Res.* **32**, 135–147 (1992).
28. Masson, G.S. & Castet, E. Parallel motion processing for the initiation of short-latency ocular following in humans. *J. Neurosci.* **22**, 5149–5163 (2002).
29. Stoner, G.R. & Albright, T.D. Neural correlates of perceptual motion coherence. *Nature* **358**, 412–414 (1992).
30. Priebe, N.J., Cassanello, C.R. & Lisberger, S.G. The neural representation of speed in macaque area MT/V5. *J. Neurosci.* **23**, 5650–5661 (2003).
31. Maunsell, J.H.R. Physiological evidence for two visual subsystems. in *Matters of Intelligence* (ed. L.M. Vaina) 59–87 (Reidel, Dordrecht, The Netherlands, 1987).
32. Raiguel, S., Lagae, L., Gulyás, B. & Orban, G.A. Response latencies of visual cells in macaque areas V1, V2, and V5. *Brain Res.* **493**, 155–159 (1989).
33. Raiguel, S.E., Xiao, D-K., Marcar, V.L. & Orban, G.A. Response latency of macaque area MT/V5 neurons and its relationship to stimulus parameters. *J. Neurophysiol.* **82**, 1944–1956 (1999).
34. Schmolesky, M.T. *et al.* Signal timing across the macaque visual system. *J. Neurophysiol.* **79**, 3272–3278 (1998).
35. Bair, W., Cavanaugh, J.R., Smith, M.A. & Movshon, J.A. The timing of response onset and offset in macaque visual neurons. *J. Neurosci.* **22**, 3189–3205 (2002).
36. Albrecht, D.G. Visual cortex neurons in monkey and cat: effect of contrast on the spatial and temporal phase transfer functions. *Vis. Neurosci.* **12**, 1191–1210 (1995).
37. Carandini, M., Heeger, D.J. & Movshon, J.A. Linearity and normalization in simple cells of the macaque primary visual cortex. *J. Neurosci.* **17**, 8621–8644 (1997).
38. Gawne, T.J., Kjaer, T.W. & Richmond, B.J. Latency: another potential code for feature binding in striate cortex. *J. Neurophysiol.* **76**, 1356–1360 (1996).
39. Basole, A., White, L.E. & Fitzpatrick, D. Mapping multiple features in the population response of visual cortex. *Nature* **423**, 986–990 (2003).
40. Gizzi, M.S., Katz, E., Schumer, R.A. & Movshon, J.A. Selectivity for orientation and direction of motion of single neurons in cat striate and extrastriate visual cortex. *J. Neurophysiol.* **63**, 1529–1543 (1990).
41. Simoncelli, E.P. & Heeger, D.J. A model of neuronal responses in visual area MT. *Vision Res.* **38**, 743–761 (1998).
42. Albrecht, D.G., Geisler, W.S., Frazor, R.A. & Crane, A.M. Visual cortex neurons of monkeys and cats: temporal dynamics of the contrast response function. *J. Neurophysiol.* **88**, 888–913 (2002).
43. Bullier, J., Hupé, J.M., James, A.C. & Girard, P. The role of feedback connections in shaping the responses of visual cortical neurons. *Prog. Brain Res.* **134**, 193–204 (2001).
44. Wilson, H.R., Ferrera, V.P. & Yo, C. A psychophysically motivated model for two-dimensional motion perception. *Vis. Neurosci.* **9**, 79–97 (1992).
45. Gegenfurtner, K.R., Kiper, D.C. & Levitt, J.B. Functional properties of neurons in macaque area V3. *J. Neurophysiol.* **77**, 1906–1923 (1997).
46. Levitt, J.B., Kiper, D.C. & Movshon, J.A. Receptive fields and functional architecture of macaque V2. *J. Neurophysiol.* **71**, 2517–2542 (1994).
47. Cavanaugh, J.R., Bair, W. & Movshon, J.A. Nature and interaction of signals from the receptive field center and surround in macaque V1 neurons. *J. Neurophysiol.* **88**, 2530–2546 (2002).
48. Gallyas, F. Silver staining of myelin by means of physical development. *Neurol. Res.* **1**, 203–209 (1979).
49. Desimone, R. & Ungerleider, L.G. Multiple visual areas in the caudal superior temporal sulcus of the macaque. *J. Comp. Neurol.* **248**, 164–189 (1986).